









Pulse- and field-resolved THz-diagnostics at 4th generation lightsources

M. CHEN,^{1,2}  J.-C. DEINERT,¹  B. GREEN,¹ Z. WANG,¹  I. ILYAKOV,¹ N. AWARI,¹  M. BAWATNA,¹ S. GERMANSKIY,¹ T. V. A. G. DE OLIVEIRA,^{1,3} G. GELONI,⁴ T. TANIKAWA,⁴ M. GENSCHE,^{2,5,6}  AND S. KOVALEV^{1,7} 

¹*Helmholtz-Zentrum Dresden-Rossendorf, Bautzner Landstr. 400, 01328 Dresden, Germany*

²*Institut für Optik und Atomare Physik, Technische Universität Berlin, Straße des 17. Juni 135, 10623 Berlin, Germany*

³*Institut für Angewandte Physik, Technische Universität Dresden, Nöthnitzer Str. 61, 01187 Dresden, Germany*

⁴*European X-ray Free-Electron Laser, Albert-Einstein-Ring 19, 22761 Hamburg, Germany*

⁵*DLR - Institute of Optical Sensor Systems, Rutherfordstr. 2, 12489 Berlin, Germany*

⁶*michael.gensch@dlr.de*

⁷*s.kovalev@hzdr.de*

Abstract: Multi-color pump-probe techniques utilizing modern accelerator-based 4th generation light sources such as X-ray free electron lasers or superradiant THz facilities have become important science drivers over the past 10 years. In this type of experiments the precise knowledge of the properties of the involved accelerator-based light pulses crucially determines the achievable sensitivity and temporal resolution. In this work we demonstrate and discuss the powerful role pulse- and field-resolved- detection of superradiant THz pulses can play for improving the precision of THz pump - femtosecond laser probe experiments at superradiant THz facilities in particular and at 4th generation light sources in general. The developed diagnostic scheme provides real-time information on the properties of individual pulses from multiple accelerator based THz sources and opens a robust way for sub femtosecond timing. Correlations between amplitude and phase of the pulses emitted from different superradiant THz sources furthermore provide insides into the properties of the driving electron bunches and is of general interest for the ultra-fast diagnostics at 4th generation light sources.

Published by The Optical Society under the terms of the [Creative Commons Attribution 4.0 License](https://creativecommons.org/licenses/by/4.0/). Further distribution of this work must maintain attribution to the author(s) and the published article's title, journal citation, and DOI.

1. Introduction

Time resolved pump-probe experiments play a key role in understanding of fundamental processes in material sciences as well as in life sciences. Utilizing modern ultra-short pulse laser system, sub-femtosecond time resolution can be achieved routinely, enabling the study of various dynamical processes of matter. At the same time, modern accelerator technology and modern light sources based on this technology have advanced to the extent that ultra-short Fourier-limited light pulses from the deep THz to the hard X-ray regime can be provided at unprecedented intensities and repetition rates. Thereby, traditionally linac-based sources of this type based on ultra-short relativistic electron bunches such as X-FELs and superradiant THz sources have been classified as 4th generation lightsources. These facilities meanwhile provide intense light pulses for user experiments to drive, probe and detect dynamics in matter on all relevant energy-, time- and length scales. One emerging new class of accelerator-driven lightsources are superradiant THz facilities [1–6]. Here, ultra-short electron bunches generate strong CEP

stable THz pulses with unique properties utilized as an intense, selective low energy excitation of matter in typical experiments [5,7–10], while the subsequent dynamics are typically probed on sub-cycle timescales utilizing appropriately synchronized and timed femtosecond laser pulses. Since the stability of accelerator-based light sources, especially with respect to timing jitter and pulse intensity, is inferior to typical optical lasers, the achievable dynamic range, precision and sensitivity depends heavily on sophisticated schemes that provide information on all relevant pulse properties [11,12]. Several prototype schemes have been successfully demonstrated, which provide pulse-resolved information and subsequent near real-time data analysis (e.g. [8]). Here we present a recent upgrade of the prototype real-time diagnostics at the superradiant THz facility TELBE [5] towards implementing pulse- and field- resolved diagnostics of two independent and conceptually different THz emitters, a coherent diffraction radiator (CDR) and an undulator. The performance of this upgrade is benchmarked by a time-domain spectroscopy experiment detecting and characterizing the THz pulses emitted from the THz undulator. The achievable temporal resolution is established and correlations between the properties of THz pulses from the CDR source and the undulator source with respect to arrival time, intensity and spectral content are discussed. The observations reveal in general that the combination of multiple pulse- and field-resolved photon diagnostics exercised on two sequential superradiant THz emitters can provide important insights into the origin of observed instabilities in the performance of 4th generation light sources. Additionally, the proposed scheme of sequential arrival time monitor provides better temporal resolution than precedented ones, as the effect of timing jitter between the two THz radiation sources is substantially reduced [13].

2. Experimental setup

The experimental setup is schematically shown in Fig. 1. It consists of two arrival-time-monitor systems (ATM) which detect the THz pulses from the CDR source and the undulator source in parallel, one pyroelectric detector to independently determine the THz intensity from the undulator, and a sequential time-domain spectroscopy set-up which serves for a the benchmark experiment.

For the optical beam, a commercial regenerative Ti:Sapphire femtosecond laser amplifier was utilized that delivers 100 fs pulses with a pulse energy of 5 μJ and a center wavelength of 800 nm at 200 kHz repetition rate. The laser system is synchronized to the accelerator using a commercial Synchrolock AP system from Coherent, Inc. and has around 500 fs timing jitter. The laser is split into three portions: one beam serves as probe in the CDR ATM, one beam serves as probe in the undulator ATM and one beam is utilized as probe laser in the benchmark time-domain spectroscopy experiment.

The fundamental principle of the ATM is a spectral decoding scheme in which the THz field is mixed with a linearly chirped few ps long optical probe beam in a ZnTe crystal [14–16] and, thereby, induces a change of the polarization state of the part of the laser pulse. The measurements are performed in the so called near-crossed-polarizer detection geometry where a pair of almost orthogonality aligned polarizer filters is placed before and after the ZnTe crystal to increase the THz-induced modulation depth and suppress the background, enabling high SNR within a single shot [15]. The time information is hence encoded in the spectrum of the linearly chirped laser pulse and mapped into space by a grating spectrometer. The achievable temporal resolution of the arrival time depends on the chirped pulse length, the timing jitter between THz and laser pulse, the bandwidth of the laser pulse and the bandwidth of the THz pulse. For typical parameters at TELBE source [5], the optimal chirped laser pulse duration is 10 ps (FWHM) for the CDR ATM, which is achieved by a grating pair stretcher. As undulator pulse has multiple cycles (see Fig. 1), we take one of the field cycle for arrival time determination, the position of which can be tracked with CDR ATM. For higher temporal resolution, we choose a shorter pulse duration for the undulator ATM as 6 ps, which is achieved by using glass rods made of NSF-6 glass. Note, that

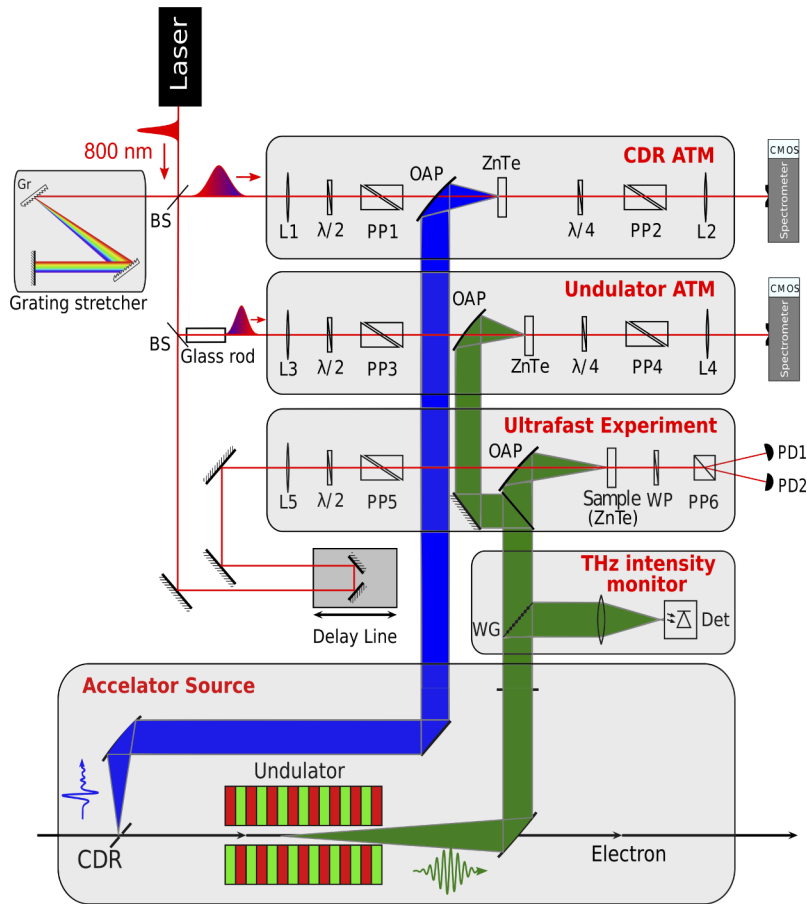


Fig. 1. Experimental scheme: The setup has been installed and tested at the TELBE THz facility which consist of two superradiant THz sources: a CDR and an undulator. Two ATMs are employed: one detecting the CDR pulses and one detecting pulses from the undulator. Additional monitor based on fast pyroelectric detector measures the intensities of each undulator pulse. Sequential EO sampling serves as ultrafast benchmark experiment.

using a chirped laser pulse shorter than 10 ps in the CDR ATM is not suitable, because it needs to be several times bigger than the total jitter including also slow drifts. For the undulator ATM the pulse duration, and thereby the time window, can be chosen shorter, as the long multi-cycle undulator pulses are less likely to completely leave this time window because of drifts.

In the benchmark experiment, the undulator was operated at a central frequency of 0.7 THz, the spectral decoding (SD) traces of both ATMs (see Figs. 2(a) and 2(b)) and the electro-optic (EO) sampling trace of the undulator pulses were measured.

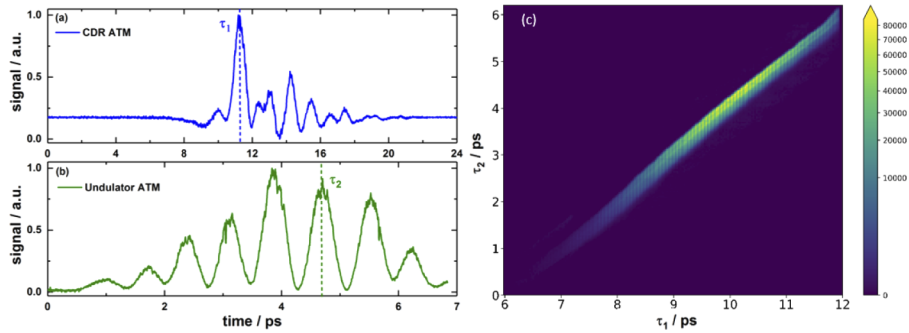


Fig. 2. Spectral-decoding electro-optic detection with the two ATMs: (a) SD trace of CDR ATM. (b) SD trace of undulator ATM. (c) 2D histogram correlating the arrival times determined by the two ATMs. Value on colour bar means number of events.

3. Data analysis procedure

The data analysis consist of three steps. The first step is arrival time determination. The arrival time of the CDR pulses τ_1 and the undulator pulses τ_2 , with respect to the laser pulses, are derived from the peak pixel position of the SD traces taken by CDR ATM and undulator ATM, respectively. The second step is to read out the undulator pulse intensity from the SD traces taken by undulator ATM to compensate for their power fluctuation. The third step is the procedure of data correction and data binning, where the timing jitter between pump and probe pulses as well as power fluctuations are corrected.

3.1. Arrival time determination

In order to deduce the pixel-to-time mapping for both arrival time monitors, a calibration procedure similar as in [8,17] is performed. The significant linear correlation between time and pixel of the CDR ATM results from the linear chirp of the probe pulses. For the CDR ATM, the primary peak in its SD trace is chosen to determine the peak shift, as shown in Fig. 2(a). The calibration rate of the CDR ATM is $\tau_1 = 11.9 \cdot P_1$, where P_1 denotes the peak position in pixels and τ_1 is the relative arrival time of CDR pulse in femtoseconds. For the undulator ATM, as shown in Fig. 2(b), one particular peak is chosen for calibration. To be able to lock to one specific peak during several hours/days, timing jitter τ_1 should be determined at first that allow us to determine the approximate position of the specific peak of the undulator, without this procedure, locking directly to the undulator pulses requires much longer chirped probe pulse that reduces temporal resolution. Moreover, since the pulse for the undulator ATM is chirped by the glass rod instead of a grating pair, second order dispersion also needs to be taken into consideration. As a result of that, a second order term is added to the pixel to time transformation. Calibrating the mapping formulae with a precise linear stage gives: $\tau_2 = \alpha \cdot P_2 - \beta \cdot P_2^2$, where P_2 and τ_2 are peak pixel position and relative arrival time of undulator pulse, with $\alpha = 4.03$, $\beta = 4.15 \times 10^{-4}$. The dependence between undulator and CDR arrival times measured for few millions pulses (a few

tens of seconds of acquisition) is shown in a 2D histogram in Fig. 2(c). It shows a quasi-linear correlation as expected, however, the small jitter between CDR and undulator pulses broadens and distorts the line.

3.2. Undulator pulses intensity determination

Apart from the arrival time, the undulator ATM provides information about the undulator pulse waveform and its amplitude, and can hence also be employed as a pulse-resolved intensity and spectrum monitor. The proportionality to intensity and not to field strength is caused by the fact that we are operating the ATM at crossed-polarization geometry, where the SD response is quadratic to the THz field strength.

3.3. Data correction and data binning

At this stage, each data point measured during the experiment is assigned to the corresponding delay between pump and probe pulses. The real time delay is comprised of (i) the delay line position, which is scanned during the measurement, and (ii) the timing jitter, determined for each pulse by the ATM. A data binning procedure is implemented by averaging all the data points that share the same time delay and belong to the same intensity levels.

4. Experimental results and discussion

To compare the performance of the sequential arrival time monitor approach with the single one [8], high-resolution time-domain spectroscopy measurements on the undulator pulse were performed. At first, we studied the performance of the pulse-to-pulse timing jitter, as shown in Fig. 3. Here, electro-optic sampling (EOS) of the undulator radiation tuned to 0.7 THz is measured and the timing jitter accuracy is determined through the width of the temporal distribution of the unbinned data (as in [6,8]). The results of EOS measurements utilizing single and double ATM are shown in Figs. 3(a) and 3(c), respectively. Here, each point represents a single event: the EOS signal amplitude for y-axis and timing for x-axis for each THz pulse at 100 kHz repetition rate. As a figure of merit of timing accuracy we use the distribution width of raw, i.e. not binned, EOS data along the time axis. To minimize the effect of intensity fluctuations on the temporal EOS distribution, we characterized the EOS distribution along the time axis when the THz field is zero (see Fig. 3(c) black box area). The temporal EOS distribution around these points is termed zero-crossing width. Width of ten zero-crossing positions were evaluated, chosen symmetrically around the strongest THz field cycle (Fig. 3(e)). As expected, the double ATM scheme improves the timing precision from around 50 fs (RMS) to around 25 fs (RMS), compared to that of the single ATM scheme under the same accelerator conditions. Thereby an almost twice better precision is achieved. We attribute this increase of accuracy to the fact that with the double ATM scheme, we can directly lock to the pulse of interest. This is the major advance in comparison with the CDR ATM monitor. For the latter, timing jitter between different accelerator based sources is not corrected, which limits the precision in time resolution [13].

In order to study the long-term performance of double ATM, data binning was applied to average out the short-term jitter and intensity fluctuations. A set of ten EOS traces was measured with ten minutes time interval between measurements Fig. 4. The long-term instabilities now can only stem from slow drifts, e.g. due to thermal drifts of the path length in the electron and photon transport beamlines.

As a measure of the drifts, we analyzed the position of the zero-crossings of the binned data. In Figs. 4(b) and 4(d), the zoom for one set around zero-crossing at 11 ps is presented for single and double ATM scheme. It is seen that drifts are significantly less for the double ATM scheme. To estimate the drifts, we measured the RMS deviation of ten zero-crossings for each set, as shown in Fig. 4(e). Similar to what has been observed on short time scales, the timing precision

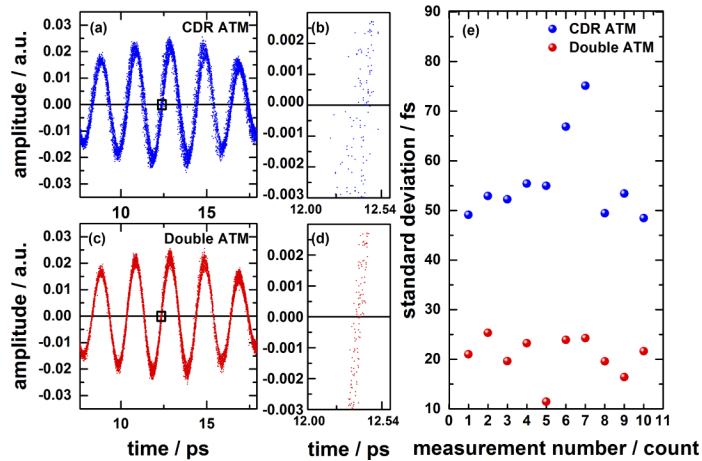


Fig. 3. Benchmark experiment - short-term performance: (a) EO sampling trace of one loop measurement after data correction with timing signal from CDR ATM and (c) from double ATM. (b) and (d) are enlarged views of one zero-crossing point, indicated by the corresponding rectangular area in (a) and (c), respectively. (e) Standard deviations of data points distribution around 10 zero-crossing positions corrected by CDR ATM and double ATM method

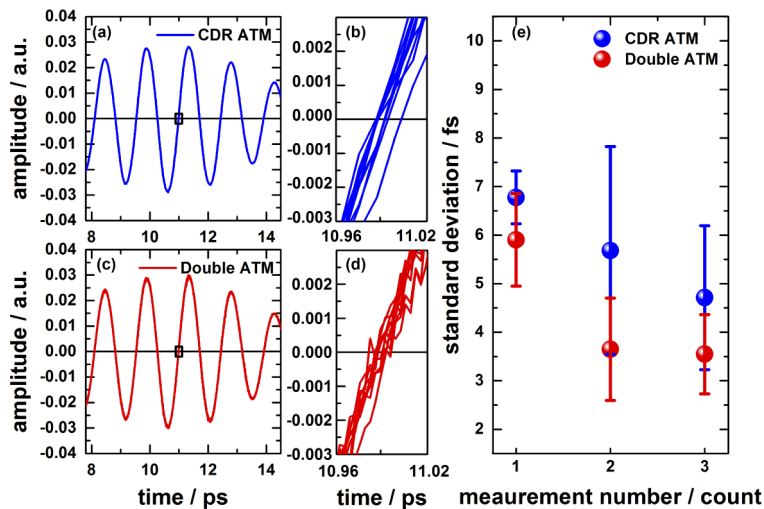


Fig. 4. Benchmark experiment - long term performance: (a) Ten EO sampling traces of measurement 1 using the single ATM timing signal. (b) Enlarged view of black rectangular area in (a). (c) Ten EO sampling traces of measurement 1 using the double ATM timing signal. (d) Enlarged view of the black rectangular area in (c). (e) Averaged standard deviation over ten zero-crossing positions of three measurements using single and double ATM scheme. Error bars originate from the distribution of the standard deviations over ten zero-crossings of each measurement.

of the double ATM scheme is significantly improved over that of the single ATM scheme and can reach values well in the sub-10 fs regime down to 3.5 fs (RMS).

As mentioned earlier, the proposed scheme also reveals a large diagnostic potential for superradiant THz sources relevant for the field of accelerator diagnostics. The full analysis of the simultaneously detected THz waveforms originating from the two independent superradiant THz emitters and the high dynamic range, high resolution time-domain spectroscopy measurements opens up interesting possibilities to correlate the observed timing and intensity instabilities. In Fig. 5 such an analysis is shown aiming for investigating whether there is a systematic correlation between intensity fluctuations of the THz undulator source and the time delay between CDR and undulator pulses. Here, we observe a strong dependence between undulator timing (relative to CDR) and its intensity variation that may originate from slight electron bunch energy variations and spatial variations of the electron bunch's trajectory. To understand these correlations further, we made use of the pulse-resolved intensity monitor to specifically evaluate correlations at different undulator THz intensity levels.

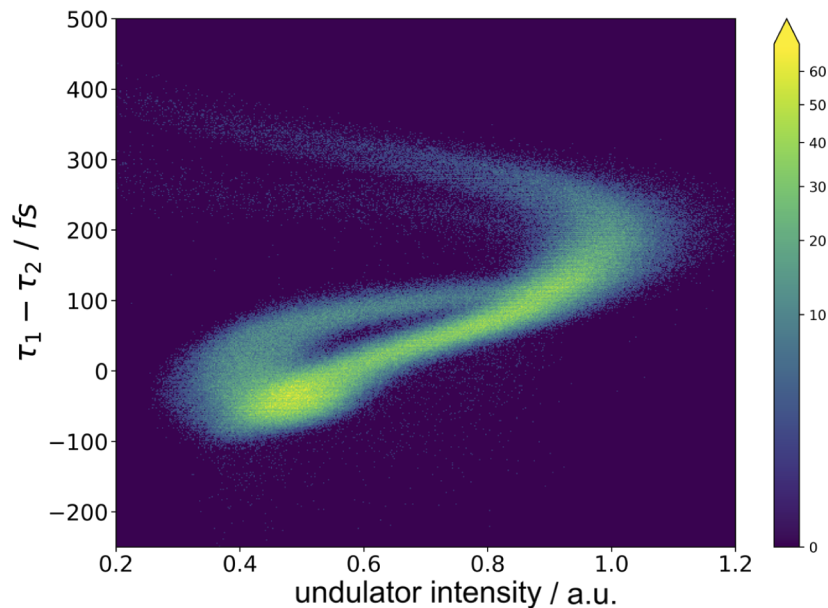


Fig. 5. Correlation between arrival time and intensity: Dependence of the arrival time difference between pulses emitted from the CDR emitter and the undulator on the undulator pulse intensity levels. A substantial nontrivial dependency is observed. Value on colour bar means number of events.

As can be seen in Figs. 6(a) and 6(b), a systematic drift of the timing of the THz undulator pulses (with respect to the CDR time stamp) towards positive time delays with decreasing intensities is observed. Further analysis shows, that by utilizing the double ATM scheme this drift can be compensated and that timing jitter resolution of actual measurements will not depend on such instabilities (see Figs. 6(c)–6(e)). Taking the analysis further, one can also look for systematic correlations between the spectral content and the intensity of the undulator radiation. The results of this analysis are shown in Fig. 7. As can be seen, the central frequency of the superradiant undulator pulses also shows a systematic dependency on pulse intensity. It shifts towards lower frequency by up to 6 GHz (0.9% from central frequency) upon decreasing intensity levels.

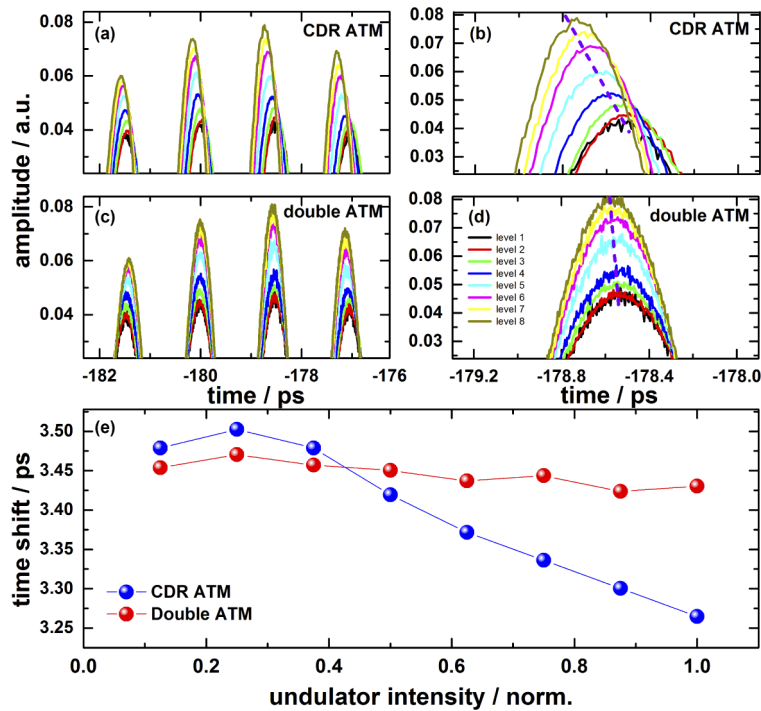


Fig. 6. Benchmark experiment – compensation of long term drifts: (a) and (c) EO sampling traces sorted with single and double ATM scheme, respectively. Both are binned with same THz intensity classification. (c) and (d) are an enlarged view of the strongest peak in (a) and (b), respectively. Purple dashed lines follow the peak position of each trace within a different THz intensity bin. (e) Dependence of the peak position in (b) and (d) on the undulator intensity.

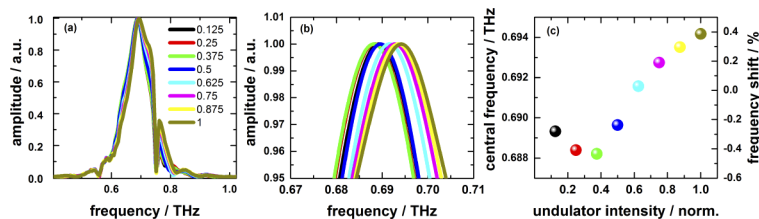


Fig. 7. Benchmark experiment – indication of electron energy drifts: (a) Spectrum of the EO sampling traces using double ATM as timing signal in different intensity level. Value in legend refers to the normalized undulator intensity level in Fig. 6(e). (b) Enlarged view of peak area. (c) Peak position in each intensity level. The THz frequency drifts by 6 GHz down with decreasing intensity levels.

The order of magnitude of the observation, (i) a decrease of the time delay between pulses from the CDR emitter and the undulator by few 100 fs, and (ii) a softening of the undulator frequency in the few percentage regime matches back of an envelope estimations well. Further investigations would be needed to prove that this scenario is correct but are beyond the scope of this article.

In summary, in this article we demonstrate the potential of pulse- and field-resolved diagnostics for superradiant THz sources utilizing a sequence of arrival time monitors for each involved

accelerator-based source. Our pulse- and field-resolved diagnostics can be directly transferred to the soft-X-ray FEL FLASH [3,18] where a THz undulator source is followed by an edge radiation source. Our findings are also of high relevance for current proposals to implement superradiant undulators into the European XFEL [19] and the LCLS-II FEL [20] as well as the many existing or discussed compact accelerator-based superradiant THz undulator facilities (see e.g. [21–24]).

Funding

Bundesministerium für Bildung und Forschung (05K16ODC); Horizon 2020 Framework Programme (654220, 737038).

Acknowledgments

The authors acknowledge the ELBE team for operating the ELBE facility.

Disclosures

The authors declare no conflicts of interest.

References

1. M. Gensch, L. Bittner, A. Chesnov, H. Delsim-Hashemi, M. Drescher, B. Faatz, J. Feldhaus, U. Fruehling, G. A. Geloni, C. Gerth, O. Grimm, U. Hahn, M. Hesse, S. Kapitzki, V. Kocharyan, O. Kozlov, E. Matyushevsky, N. Morozov, D. Petrov, E. Ploenjes, M. Roehling, J. Rossbach, E. L. Saldin, B. Schmidt, P. Schmueser, E. A. Schneidmiller, E. Syresin, A. Willner, and M. V. Yurkov, "New infrared undulator beamline at FLASH," *Infrared Phys. Technol.* **51**(5), 423–425 (2008).
2. Z. Wu, A. S. Fisher, J. Goodfellow, M. Fuchs, D. Daranciang, M. Hogan, H. Loos, and A. Lindenberg, "Intense terahertz pulses from SLAC electron beams using coherent transition radiation," *Rev. Sci. Instrum.* **84**(2), 022701 (2013).
3. N. Stojanovic and M. Drescher, "Accelerator- and laser-based sources of high-field terahertz pulses," *J. Phys. B: At., Mol. Opt. Phys.* **46**(19), 192001 (2013).
4. A. Perucchi, S. Di Mitri, G. Penco, E. Allaria, and S. Lupi, "The TeraFERMI terahertz source at the seeded FERMI free-electron-laser facility," *Rev. Sci. Instrum.* **84**(2), 022702 (2013).
5. B. Green, S. Kovalev, V. Asgekar, G. Geloni, U. Lehnert, T. Golz, M. Kuntzsch, C. Bauer, J. Hauser, J. Voigtlaender, B. Wustmann, I. Koesterke, M. Schwarz, M. Freitag, A. Arnold, J. Teichert, M. Justus, W. Seidel, C. Ilgner, N. Awari, D. Nicoletti, S. Kaiser, Y. Laplace, S. Rajasekaran, L. Zhang, S. Winnerl, H. Schneider, G. Schay, I. Lorincz, A. A. Rauscher, I. Radu, S. Mahrlein, T. H. Kim, J. S. Lee, T. Kampfrath, S. Wall, J. Heberle, A. Malnasi-Csizmadia, A. Steiger, A. S. Muller, M. Helm, U. Schramm, T. Cowan, P. Michel, A. Cavalleri, A. S. Fisher, N. Stojanovic, and M. Gensch, "High-Field High-Repetition-Rate Sources for the Coherent THz Control of Matter," *Sci. Rep.* **6**(1), 22256 (2016).
6. R. Pan, E. Zapolnova, T. Golz, A. J. Krmpot, M. D. Rabasovic, J. Petrovic, V. Asgekar, B. Faatz, F. Tavella, A. Perucchi, S. Kovalev, B. Green, G. Geloni, T. Tanikawa, M. Yurkov, E. Schneidmiller, M. Gensch, and N. Stojanovic, "Photon diagnostics at the FLASH THz beamline," *J. Synchrotron Radiat.* **26**(3), 700–707 (2019).
7. J. L. Larue, T. Katayama, A. Lindenberg, A. S. Fisher, H. Öström, A. Nilsson, and H. Ogasawara, "THz-Pulse-Induced Selective Catalytic CO Oxidation on Ru," *Phys. Rev. Lett.* **115**(3), 036103 (2015).
8. S. Kovalev, B. Green, T. Golz, S. Mahrlein, N. Stojanovic, A. S. Fisher, T. Kampfrath, and M. Gensch, "Probing ultra-fast processes with high dynamic range at 4th-generation light sources: Arrival time and intensity binning at unprecedented repetition rates," *Struct. Dyn.* **4**(2), 024301 (2017).
9. H. A. Hafez, S. Kovalev, J. C. Deinert, Z. Mics, B. Green, N. Awari, M. Chen, S. Germanskiy, U. Lehnert, J. Teichert, Z. Wang, K. J. Tielrooij, Z. Liu, Z. Chen, A. Narita, K. Müllen, M. Bonn, M. Gensch, and D. Turchinovich, "Extremely efficient terahertz high-harmonic generation in graphene by hot Dirac fermions," *Nature* **561**(7724), 507–511 (2018).
10. Z. Wang, S. Kovalev, N. Awari, M. Chen, S. Germanskiy, B. Green, J.-C. Deinert, T. Kampfrath, J. Milano, and M. Gensch, "Magnetic field dependence of antiferromagnetic resonance in NiO," *Appl. Phys. Lett.* **112**(25), 252404 (2018).
11. J. M. Glownia, J. Cryan, J. Andreasson, A. Belkacem, N. Berrah, C. I. Blaga, C. Bostedt, J. Bozek, L. F. DiMauro, L. Fang, J. Frisch, O. Gessner, M. Gühr, J. Hajdu, M. P. Hertlein, M. Hoener, G. Huang, O. Kornilov, J. P. Marangos, A. M. March, B. K. McFarland, H. Merdji, V. S. Petrovic, C. Raman, D. Ray, D. A. Reis, M. Trigo, J. L. White, W. White, R. Wilcox, L. Young, R. N. Coffee, and P. H. Bucksbaum, "Time-resolved pump-probe experiments at the LCLS," *Opt. Express* **18**(17), 17620–17630 (2010).
12. E. Savelyev, R. Boll, C. Bomme, N. Schirmel, H. Redlin, B. Erk, S. Düsterer, E. Müller, H. Höppner, S. Toleikis, J. Müller, M. Kristin Czwilinna, R. Treusch, T. Kierspel, T. Mullins, S. Trippel, J. Wiese, J. Küpper, F. Braue,

- F. Krecinic, A. Rouzée, P. Rudawski, P. Johnsson, K. Amini, A. Lauer, M. Burt, M. Brouard, L. Christensen, J. Thøgersen, H. Stapelfeldt, N. Berrah, M. Müller, A. Ulmer, S. Techert, A. Rudenko, and D. Rolles, "Jitter-correction for IR/UV-XUV pump-probe experiments at the FLASH free-electron laser," *New J. Phys.* **19**(4), 043009 (2017).
13. F. Tavella, N. Stojanovic, G. Geloni, and M. Gensch, "Few-femtosecond timing at fourth-generation X-ray light sources," *Nat. Photonics* **5**(3), 162–165 (2011).
 14. Z. Jiang and X.-C. Zhang, "Electro-optic measurement of THz field pulses with a chirped optical beam," *Appl. Phys. Lett.* **72**(16), 1945–1947 (1998).
 15. Z. Jiang, F. G. Sun, Q. Chen, and X. C. Zhang, "Electro-optic sampling near zero optical transmission point," *Appl. Phys. Lett.* **74**(9), 1191–1193 (1999).
 16. G. Berden, S. P. Jamison, A. M. MacLeod, W. A. Gillespie, B. Redlich, and A. F. G. Van der Meer, "Electro-optic technique with improved time resolution for real-time, nondestructive, single-shot measurements of femtosecond electron bunch profiles," *Phys. Rev. Lett.* **93**(11), 114802 (2004).
 17. M. R. Bionta, N. Hartmann, M. Weaver, D. French, D. J. Nicholson, J. P. Cryan, J. M. Glowina, K. Baker, C. Bostedt, M. Chollet, Y. Ding, D. M. Fritz, A. R. Fry, D. J. Kane, J. Krzywinski, H. T. Lemke, M. Messerschmidt, S. Schorb, D. Zhu, W. E. White, and R. N. Coffee, "Spectral encoding method for measuring the relative arrival time between x-ray/optical pulses," *Rev. Sci. Instrum.* **85**(8), 083116 (2014).
 18. K. Tiedtke, A. Azima, N. Von Bargen, L. Bittner, S. Bonfigt, S. Düsterer, B. Faatz, U. Frühling, M. Gensch, C. Gerth, N. Guerassimova, U. Hahn, T. Hans, M. Hesse, K. Honkavaara, U. Jastrow, P. Juranic, S. Kapitzki, B. Keitel, T. Kracht, M. Kuhlmann, W. B. Li, M. Martins, T. Núñez, E. Plönjes, H. Redlin, E. L. Saldin, E. A. Schneidmiller, J. R. Schneider, S. Schreiber, N. Stojanovic, F. Tavella, S. Toleikis, R. Treusch, H. Weigelt, M. Wellhöfer, H. Wabnitz, M. V. Yurkov, and J. Feldhaus, "The soft x-ray free-electron laser FLASH at DESY: Beamlines, diagnostics and end-stations," *New J. Phys.* **11**(2), 023029 (2009).
 19. T. Tanikawa, S. Karabekyan, S. Kovalev, S. Casalbuoni, V. Asgekar, S. Serkez, G. Geloni, and M. Gensch, "A superradiant THz undulator source for XFELs," *J. Instrum.* **14**(05), P05024 (2019).
 20. Z. Huang, A. Fisher, M. Hoffmann, B. Jacobson, and Z. Zhang, "A high-power, high-repetition rate THz source for LCLS-II pump-probe experiments," in presented in *39th International Free-Electron Laser Conference*, (Hamburg, Germany, 2019).
 21. M. C. Chou, K. T. Hsu, S. Y. Hsu, N. Y. Huang, C. S. Hwang, J. Y. Hwang, J. C. Jan, C. K. Kuan, W. K. Lau, A. P. Lee, C. C. Liang, G. H. Luo, I. C. Sheng, and Y. H. Wen, "First observation of coherent THz undulator radiation driven by NSRRC high brightness photo-injector," in *Proceedings of 38th International Free Electron Laser Conference*, K. Bishofberger, ed. (Santa Fe, NM, USA, 2017), p. MOP052.
 22. S. Suphakul, H. Zen, T. Kii, and H. Ohgaki, "Measurement of Coherent Undulator Radiation of Compact Terahertz Radiation Source at Kyoto University," *Int. J. Magnetism Electromagnetism* **3**(1), 1–7 (2017).
 23. N. Chaisueb, S. Chunjarean, C. Thongbai, and S. Rimjaem, "Development of a compact electromagnetic undulator for linac-based coherent THz radiation source in Thailand," *Nucl. Instrum. Methods Phys. Res., Sect. A* **902**, 1–8 (2018).
 24. V. Sahakyan, A. A. Sargsyan, G. Zanyan, T. Vardanyan, B. Grigoryan, and V. Tsakanov, "Middle Infrared and THz Sources at AREAL," *Arm. J. Phys.* **11**, 111–116 (2018).